The Journal of Chemical Physics

On the role of non-diagonal system–environment interactions in bridge-mediated electron transfer

Cite as: J. Chem. Phys. **153**, 185101 (2020); https://doi.org/10.1063/5.0027976
Submitted: 01 September 2020 • Accepted: 25 October 2020 • Published Online: 10 November 2020

Nirmalendu Acharyya, Roman Ovcharenko and Benjamin P. Fingerhut

The Journal of Chemical Physics ARTICLE scitation.org/journal/jcp

On the role of non-diagonal system–environment interactions in bridge-mediated electron transfer

Cite as: J. Chem. Phys. 153, 185101 (2020); doi: 10.1063/5.0027976
Submitted: 1 September 2020 • Accepted: 25 October 2020 •
Published Online: 10 November 2020

Nirmalendu Acharyya, Roman Ovcharenko, and Benjamin P. Fingerhut[a)]

AFFILIATIONS

Max-Born-Institut für Nichtlineare Optik und Kurzzeitspektroskopie, D-12489 Berlin, Germany

Note: This paper is part of the JCP Special Topic on Excitons: Energetics and Spatio-Temporal Dynamics.
[a)]**Author to whom correspondence should be addressed:** fingerhut@mbi-berlin.de

ABSTRACT

Bridge-mediated electron transfer (ET) between a donor and an acceptor is prototypical for the description of numerous most important ET scenarios. While multi-step ET and the interplay of sequential and direct superexchange transfer pathways in the donor–bridge–acceptor (D–B–A) model are increasingly understood, the influence of off-diagonal system–bath interactions on the transfer dynamics is less explored. Off-diagonal interactions account for the dependence of the ET coupling elements on nuclear coordinates (non-Condon effects) and are typically neglected. Here, we numerically investigate with quasi-adiabatic propagator path integral simulations the impact of off-diagonal system–environment interactions on the transfer dynamics for a wide range of scenarios in the D–B–A model. We demonstrate that off-diagonal system–environment interactions can have profound impact on the bridge-mediated ET dynamics. In the considered scenarios, the dynamics itself does not allow for a rigorous assignment of the underlying transfer mechanism. Furthermore, we demonstrate how off-diagonal system–environment interaction mediates anomalous localization by preventing long-time depopulation of the bridge B and how coherent transfer dynamics between donor D and acceptor A can be facilitated. The arising non-exponential short-time dynamics and coherent oscillations are interpreted within an equivalent Hamiltonian representation of a primary reaction coordinate model that reveals how the complex vibronic interplay of vibrational and electronic degrees of freedom underlying the non-Condon effects can impose donor-to-acceptor coherence transfer on short timescales.

I. INTRODUCTION

Photosynthetic solar energy conversion relying on molecular charge carriers starts with the light-induced generation of Frenkel-type excitons, followed by the irreversible fixation of excitonic energy in multi-step electron transfer (ET) reactions. In reaction centers (RC) of purple bacteria or plants, the irreversible fixation proceeds across a phospholipid membrane in a sequence of directional and highly efficient ET reactions, mediated by spatially well organized (bacterio-) chlorophyll and pheophytin molecules. Pioneering electrostatic considerations,[1] supported by multi-objective evolutionary algorithm optimizations[2] suggest that efficient and irreversible charge separation requires a sequence of at least three molecular charge carriers. The emerging prototypical setup of bridge *B* mediated multi-step or superexchange ET between a donor *D* and an acceptor *A* (see Fig. 1) thus serves as a minimal model for the description of charge separation in RC and has shown relevance for numerous bridge-mediated ET processes.[3–8]

While nonadiabatic ET theory provides a valuable starting point for the descriptions of multi-step ET reactions, e.g., in the ET kinetics of the bacterial RC,[9–12] limitations arise from the inherent assumptions of instantaneous medium relaxation, the perturbative nature of Fermi golden rule expressions, and the typically neglected dependence of electronic coupling on nuclear coordinates (Condon approximation). Non-exponential short-time dynamics and coherent oscillations observed in pump–probe and, more recently,

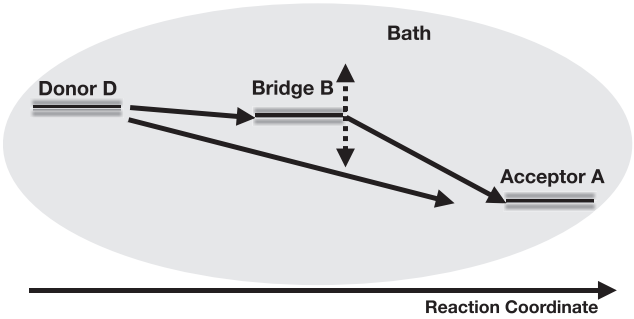

FIG. 1. Schematic of the Donor–Bridge–Acceptor (D–B–A) model. The variation of the bridge energy ϵ_B allows us to tune between the sequential D–B–A model with a low energy bridge state ($\epsilon_D > \epsilon_B$) and the D–B–A model with asymmetric-Λ configuration ($\epsilon_D < \epsilon_B$). Possible transfer pathways are the sequential $|D\rangle \rightarrow |B\rangle \rightarrow |A\rangle$ and the direct superexchange pathway $|D\rangle \rightarrow |A\rangle$. Diagonal and off-diagonal system–bath interactions lead to fluctuations of state energies ϵ_i and electron transfer coupling elements V_{ij} that mediate the dynamics.

two-dimensional electronic spectroscopy experiments of bacterial RC suggest a more complex picture where details of the ET reaction are potentially affected by the interplay of coherent electronic and nuclear motion.[13–16]

Particular theoretical challenges arise for a strong interaction of vibrational modes and electronic degrees of freedom that can impose oscillatory dynamics in bridge mediated ET.[15] Tanimura investigated multistate ET for a system coupled to a heat bath with a non-Ohmic spectral density with the numerically exact reduced hierarchy equations of motion (HEOM) approach[17,18] that is numerically efficient for Debye spectral densities. Nevertheless, the strong coupling to the environment as typically realized in ET reactions is a persistent challenge for convergence.[19,20] Pioneering quasi-adiabatic propagator path integral (QUAPI) simulations by Makri and coworkers provided valuable insight into details of ET in bacterial RC.[21,22] The QUAPI method formally does not assume a particular form of the environment spectral density or the interaction strength, but the long system–bath memory times of a sluggish environment pose persistent challenges to QUAPI methods.[23–25]

Recently, we investigated bridge-mediated ET in a model of the bacterial RC, where charge separation is initiated from a non-equilibrium excitonic superposition.[26] The path integral simulations with particularly longtime system–environment correlations allowed us to explore the influence of discrete vibrational modes on the transfer dynamics. While excitonic energy transfer was found to be strongly affected, the kinetics of ET dynamics appeared exceptionally robust to the details of the spectral density function, suggesting a picture where intramolecular vibrations assure the robustness of optimal, non-activated ET reactions.

Hence, multi-step ET in the Donor–Bridge–Acceptor (D–B–A) model is increasingly understood beyond perturbative approaches and for various (non-equilibrium) conditions of the environment. Nevertheless, the impact of off-diagonal system–bath interactions on the transfer dynamics is less explored. Such off-diagonal system–environment interactions are associated with non-Condon effects, i.e., the dependence of the coupling matrix element mediating the transfer dynamics on the nuclear coordinates. The nuclear coordinate dependence of electronic coupling was explored in the context of nonadiabatic transitions, indicating that promoting modes can dominate the vibrational effects.[27] Milischuk and Matyushov explored non-Condon effects for nonadiabatic electron transfer reactions in donor–bridge–acceptor systems.[28] The importance of non-Condon effects was further highlighted for ET at oligothiophene–fullerene interfaces via multi-layer Multi-Configuration Time-Dependent Hartree (MCTDH) simulations,[29] and the role of off-diagonal couplings was emphasized for the formation of charge-transfer states in polymeric solar cells.[30] Condensed phase ET beyond the Condon approximation was recently explored by Mavros *et al.*[31] Off-diagonal environment fluctuations were further identified to induce unexpectedly fast Förster resonant energy transfer between orthogonal oriented photoexcited molecules.[32] A review highlighting limitation of the Condon approximation in biological and bioinspired ET reactions is given in Ref. 33.

Here, we show via non-perturbative QUAPI simulations that non-diagonal system–environment interactions can have profound impact on bridge-mediated ET dynamics. We investigate the dynamics in different regimes of the prototypical Donor–Bridge–Acceptor (D–B–A) model and demonstrate that induced by non-Condon effects, the dynamics itself precludes a rigorous assignment of the underlying transfer mechanism. Furthermore, we demonstrate how anomalous localization mediated by off-diagonal system–environment interaction prevents the depopulation of the bridge B and how coherent transfer between the donor D and acceptor A can be facilitated in the presence of off-diagonal system–environment interactions.

II. THEORETICAL METHODS

A. Multi-step electron transfer with non-diagonal system–environment interaction

We consider a three-state D–B–A model (see the schematic in Fig. 1) that interacts bilinearly via diagonal and off-diagonal interactions with the environment,

$$H = \begin{pmatrix} \epsilon_D & V_{DB} & 0 \\ V_{DB} & \epsilon_B & V_{BA} \\ 0 & V_{BA} & \epsilon_A \end{pmatrix} + \sum_j \left(\frac{p_j^2}{2m_j} + m_j \omega_j^2 x_j^2 \right) + \begin{pmatrix} d_1 & C_{12} & 0 \\ C_{12} & d_2 & C_{23} \\ 0 & C_{23} & d_3 \end{pmatrix} \sum_j c_j x_j. \quad (1)$$

In Eq. (1), ϵ_i denote site energies of the donor D, bridge B, and acceptor A and V_{ij} are the respective electron transfer coupling elements. The bath is composed of harmonic oscillators with momenta p_j, position x_j, mass m_j, and frequency ω_j. The linear coupling constant c_j mediates the interaction between the system and the environment, where d_i specify the diagonal system–bath interaction inducing fluctuation of energy levels ϵ_i and C_{ij} represent off-diagonal system–bath interactions that induce fluctuations of the transfer coupling elements V_{ij}. We restrict the Hamiltonian [Eq. (1)] to the case with $V_{DA} = 0$, i.e., for diagonal system–environment interaction only, the sequential pathway contributes to the dynamics.

We consider the coupling to a single bath affecting site energies ϵ_i and transfer couplings V_{ij}. For linear coupling, all information about the environment is contained in the spectral density,

$$J(\omega) = \sum_j \frac{c_j^2}{m_j\omega_j}\delta(\omega - \omega_j). \tag{2}$$

For Ohmic dissipation,

$$J(\omega) = \frac{\alpha\pi}{2}\omega e^{-\omega/\omega_c}, \tag{3}$$

where α characterizes the system–bath interaction strength and ω_c specifies the cut-off frequency that is related to the inverse Drude memory time $\tau_D = 1/\omega_c$. A key quantity in the description of ET is the reorganization energy λ_R, defined as $\lambda_R = \frac{1}{\pi}\int \frac{J(\omega)}{\omega}d\omega \approx \alpha\omega_c/2$.

B. Primary reaction coordinate model

The Hamiltonian with bi-linear diagonal and off-diagonal system–environment interactions [Eq. (1)] can be equivalently mapped onto a model where the electronic system interacts with a primary reaction coordinate Q, which couples and dissipates into a bath[20,34,35]

$$\begin{aligned} H = &\begin{pmatrix} \epsilon_D & V_{DB} & 0 \\ V_{DB} & \epsilon_B & V_{BA} \\ 0 & V_{BA} & \epsilon_A \end{pmatrix} \\ &+ \begin{pmatrix} \kappa_1 & \Lambda_{12} & 0 \\ \Lambda_{12} & \kappa_2 & \Lambda_{23} \\ 0 & \Lambda_{23} & \kappa_3 \end{pmatrix}\sqrt{\Omega}Q + \frac{P^2}{2} + \frac{\Omega^2}{2}Q^2 \\ &+ \frac{1}{2}\sum_j \left(\frac{p_j^2}{m_j} + m_j\omega_j^2\left(q_j + \frac{\widehat{c}_i Q}{m_i\omega_i^2}\right)^2 \right). \end{aligned} \tag{4}$$

Here, Ω is the frequency of the primary mode and P is the conjugate momenta. The representation of the original Hamiltonian with diagonal and off-diagonal interactions in the form of the primary reaction coordinate model [Eq. (4)] directly reveals the coordinate dependence of transfer coupling elements V_{ij}, i.e., non-Condon effects.

The information about the interaction of the primary mode with the environment is contained in the modified spectral density,

$$\widehat{J}(\omega) = \sum_i \frac{\widehat{c}_i^2}{m_i\omega_i}\delta(\omega - \omega_i). \tag{5}$$

When the relaxation dynamics of the bath is fast, the low frequency part of $\widehat{J}(\omega)$ becomes relevant, which yields an Ohmic spectral density

$$\widehat{J}(\omega) = \gamma\omega, \tag{6}$$

where γ is the damping coefficient of the primary mode.

The primary mode can be expressed as a linear combination of the bath normal modes $\{x_j\}$,[36]

$$Q = \sum_j v_j x_j. \tag{7}$$

Using this canonical transformation [Eq. (7)], the Hamiltonian of the primary reaction coordinate model [Eq. (4)] can be recast in the form of Eq. (1) where

$$\begin{aligned} &d_1\ c_j = \sqrt{\Omega}\kappa_1 v_j, \quad d_2\ c_j = \sqrt{\Omega}\kappa_2 v_j, \quad d_3\ c_j = \sqrt{\Omega}\kappa_3 v_j, \\ &C_{12}\ c_j = \sqrt{\Omega}\Lambda_{12} v_j, \quad C_{23}\ c_j = \sqrt{\Omega}\Lambda_{23} v_j. \end{aligned} \tag{8}$$

Let us denote the eigenvalues of the interaction matrix [second term in Eq. (4)] as $\{e_1, e_2, e_3\}$. In the overdamped limit, $\gamma \gg \Omega$, the parameters of the spectral density $J(\omega)$ [Eq. (3)] are determined by

$$\omega_c \approx \frac{\Omega^2}{\gamma}, \qquad \alpha \approx \frac{e_1\gamma}{D_1\Omega^3}, \tag{9}$$

where D_1 denotes the lowest eigenvalue of the original system–bath interaction matrix [see below, Eq. (14)]. On the other hand, a diagonal shift $d_1 \to d_1 + d_0$, $d_2 \to d_2 + d_0$, and $d_3 \to d_3 + d_0$ (with d_0 being a real constant) induces a shift of the eigenvalues. In the reaction coordinate model, this corresponds to the shifting of the origin of the primary oscillator and the displacement of the initial wavepacket via κ_i. Thus, $d_0 \neq 0$ implies a displacement of an initial wavepacket from the Frank–Condon region $Q = 0$, which can be used to reveal non-Condon effects in the dynamics (cf. Sec. III D).

C. Quasi adiabatic propagator path integral simulations with non-diagonal system–environment interaction

We are interested in the time evolution of the reduced density matrix

$$\widetilde{\rho}(t) = Tr_B\left[e^{-iHt}\rho(0)e^{iHt}\right], \tag{10}$$

with H given by Eq. (1), which determines observables. For diagonal interaction with the environment ($C_{ij} = 0$), numerical exact simulations are facilitated with the QUAPI method.[37–39] For the general interaction matrix,

$$M \equiv \begin{pmatrix} d_1 & C_{12} & 0 \\ C_{12} & d_2 & C_{23} \\ 0 & C_{23} & d_3 \end{pmatrix}, \tag{11}$$

which satisfies

$$Mv_1 = D_1 v_1, \quad Mv_2 = D_2 v_2, \quad Mv_3 = D_2 v_3, \tag{12}$$

we define the unitary matrix U

$$U = [v_1, v_2, v_3], \tag{13}$$

which diagonalizes the system–bath interaction M,[40]

$$U^\dagger M U = \begin{pmatrix} D_1 & 0 & 0 \\ 0 & D_2 & 0 \\ 0 & 0 & D_3 \end{pmatrix}. \tag{14}$$

Upon transformation of the total Hamiltonian [Eq. (1)], we obtain

$$H' = U^\dagger H U \tag{15}$$

$$= U^\dagger \begin{pmatrix} \epsilon_D & V_{DB} & 0 \\ V_{DB} & \epsilon_B & V_{BA} \\ 0 & V_{BA} & \epsilon_A \end{pmatrix} U + \sum_j \left(\frac{p_j^2}{2m_j} + m_j \omega_j^2 x_j \right)$$

$$+ \begin{pmatrix} D_1 & 0 & 0 \\ 0 & D_2 & 0 \\ 0 & 0 & D_3 \end{pmatrix} \sum_j c_j x_j. \tag{16}$$

The assumption of a single spectral density affecting diagonal and off-diagonal elements of the Hamiltonian [Eq. (1)] facilitates accurate QUAPI simulations for diagonal and off-diagonal system–bath interactions via unitary transformation. This situation corresponds to the physical situation of an avoided crossing along a primary reaction coordinate with fluctuating barrier. In the current approach, the fluctuations in the site energies ϵ_i and transfer couplings V_{ij} are correlated, and the results depend on the relative sign of off-diagonal environment interactions C_{ij}. Correlation of fluctuations of site energies and transfer couplings was suggested in simulations of the Fenna-Matthews-Olson (FMO) light-harvesting complex[41] and can introduce interesting transport phenomena, as suggested in the context of a rocking ratchet driven by a single periodic force.[42] The more general case with two spectral densities acting on diagonal and off-diagonal elements of the Hamiltonian [Eq. (1)][43] was considered in Ref. 31 and was recently demonstrated for path integral approaches;[44] it enables the emergence of conical intersections.[45] Note that the unitary transformation [Eq. (16)] is determined by details of the system-environment interaction and does not necessarily diagonalize the system Hamiltonian. The introduced basis rotation is thus distinct from transformations solely determined by the system Hamiltonian.[46]

Employing factorized initial conditions $\widetilde{\rho}(0) = |D\rangle\langle D|$ and assuming the bath in thermal equilibrium at temperature T, $\widetilde{\rho}(t)$ was evaluated numerically by transforming the initial conditions

$$\rho'(t=0) = U^\dagger \rho(t=0) U, \tag{17}$$

followed by solving for $\rho'(t)$ in the transformed basis using QUAPI methods and followed by reverse transform to obtain $\widetilde{\rho}(t)$. In particular, numerical propagation was performed with the recently introduced mask assisted coarse graining of the influence coefficient (MACGIC)-QUAPI[23] method that facilitates the numerical treatment of long-time non-Markovian system–bath correlations while retaining convergence to numerical exact results. The algorithm uses a coarse grained representation of the influence functional (represented by a mask of size k_{eff}) to select the relevant paths for propagation for a finite non-Markovian memory time $\tau_M \propto \tau_D$. Convergence to numerically exact results is obtained by decreasing the size of the Trotter time-step Δt and increasing memory time $\tau_M = \Delta k_{max} \Delta t$ together with the increase in the number of coarse grained quadrature points ($k_{eff} \to \Delta k_{max}$), and details of the MACGIC-QUAPI are described in Refs. 23 and 26.

In the numerical simulations, the employed Ohmic spectral density with exponential high-frequency cutoff [Eq. (3)] accounts for non-Markovian system–bath correlations on a timescale $\tau_M \approx 100$ fs–120 fs ($\Delta k_{max} = 32$–64). Convergence is typically achieved with $k_{eff} \approx 12$, demonstrating the numerical efficiency of the MACGIC-QUAPI[23] method (see Table S.3 and Fig. S.4 of the supplementary material for numerical demonstrations of convergence). Particular challenges to the numerical treatment arise from the unitary transformation [Eq. (16)], where substantially large interstate electronic couplings can arise in the intermediate transformed basis for suitable rotation angles imposed by the system–environment interaction matrix. The substantial interstate couplings impose the necessity of small propagation time steps Δt for which longtime system–bath correlations are challenging for convergence [e.g., for typical bridge–acceptor energy gaps of 1000 cm^{-1} (see below), V'_{BA} can reach 1000 cm^{-1}, thereby inducing ultrafast coherence transfer dynamics]. Typical simulations with diagonal system–environment interaction use filter thresholds $\theta = 10^{-7}$–10^{-8} (Table S.3), account for $\approx 10^4$–10^5 paths during propagation, and show typical run times of a few minutes. For off-diagonal system–environment interaction, the number of considered paths increases to $\approx 10^5$–10^6 with run times on the order of hours. Convergence tests employed stricter filter thresholds ($\theta = 10^{-10}$) and accounted for $\approx 10^7$ paths, requiring 12 h (20 cores). Notable exceptions are the numerical simulations of anomalous bridge localization (Sec. III C) and the demonstration of direct donor–acceptor coherence transfer (Sec. III D) that require considering ultralong memory times up to ≈1 ps and 320 fs (see Table S.3 of the supplementary material), respectively, where in the case of direct donor–acceptor coherence transfer, the memory time has to cover the entire non-Markovian oscillatory dynamics.

III. RESULTS AND DISCUSSION

In the following, we investigate the impact of non-diagonal system–bath interactions on the prototypic dynamics of multi-step electron transfer in the bridge-mediated three level system (see Fig. 1). We start by investigating the regime of sequential, bridge-mediated transfer dynamics (Sec. III A) and further examine how off-diagonal system-bath interactions can activate the direct superexchange transfer pathway $|D\rangle \to |A\rangle$ (Sec. III B). Section III C presents scenarios on how off-diagonal system–bath interactions can induce anomalous population localization in the bridge state B, and Sec. III D demonstrates off-diagonal mediated coherence transfer between donor and acceptor states.

A. Sequential donor–bridge–acceptor (D–B–A) model

1. Sequential ET via a low-energy bridge ($\epsilon_D > \epsilon_B$)

We start by briefly summarizing the well-known dynamics in the sequential D–B–A model of multi-step electron transfer (Fig. 2; $\epsilon_D = 0$, $\epsilon_B = -150$ cm^{-1}, and $\epsilon_A = -1000$ cm^{-1}) with diagonal system–bath interaction [cf. Eq. (11); $d_1 = 2$, $d_2 = 1$, $d_3 = 0$, and $C_{12} = C_{23} = 0$, and simulation parameters are summarized in Tables S.1–S.3 of the supplementary material] that resembles ET in the bacterial RC.[12,22,47] For the appreciable electronic couplings ($V_{DB} = 22$ cm^{-1} < $V_{BA} = 45$ cm^{-1}), the charge transfer dynamics is characterized by low-picosecond donor D to bridge B dynamics, followed by faster sub-ps bridge B to acceptor A population transfer. The strong

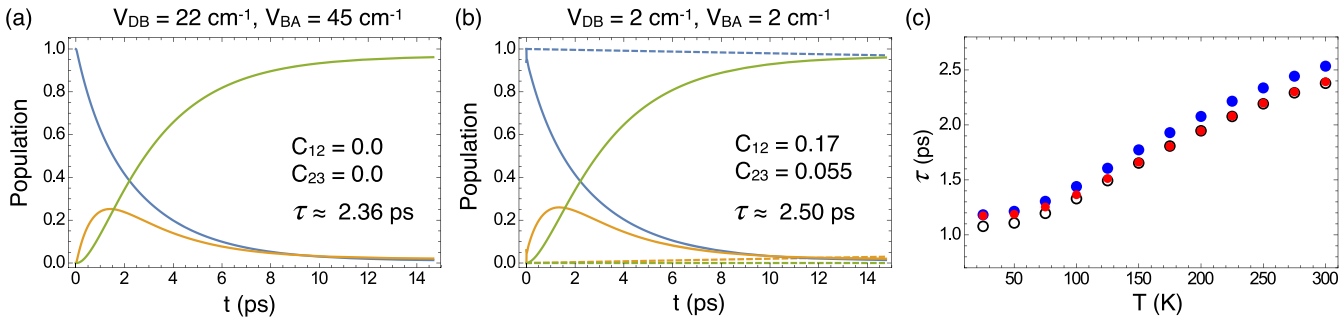

FIG. 2. Dynamics of the sequential D–B–A model (ϵ_D = 0.0, ϵ_B = −150 cm^{-1}, and ϵ_A = −1000 cm^{-1}) without (a) and with off-diagonal system–environment interaction (b) at T = 300 K. Blue, orange, and green lines represent donor D, bridge B, and acceptor A populations, respectively. Lifetime τ was obtained by an exponential fit of the donor D population dynamics. (c) Temperature dependence of the donor D population lifetime τ. Black and red symbols mark simulations without (a) and with off-diagonal system–environment interaction (b), respectively. Blue symbols mark simulations with off-diagonal system–environment interaction, but increased bridge–acceptor couplings V_{BA} = 20 cm^{-1} (see Fig. S.1 of the supplementary material). Simulation parameters are summarized in Tables S.1–S.3 of the supplementary material (see also Fig. S.3 for the impact of long-time system–bath memory on the dynamics).

coupling to the environment (λ_R = 501 cm^{-1}) is reflected in incoherent population dynamics. Despite the faster second transfer step, intermediate bridge population ≈25% is observed. The initial donor-to-bridge charge transfer dynamics is characterized by an effective time constant $\tau \approx 2.36$ ps (single exponential fit). As expected, for reduced electronic couplings, the charge transfer dynamics is substantially decelerated, now occurring on a ≈100 ps timescale [dashed lines in Fig. 2(b); V_{DB} = 2 cm^{-1} ≤ V_{BA} = 2 − 20 cm^{-1}, and see also Fig. S.1 of the supplementary material].

Off-diagonal system–environment interaction can profoundly alter this scenario [solid lines in Fig. 2(b); $C_{12} \neq 0$ and $C_{23} \neq 0$]. We find that the decay dynamics of the initially populated donor state D can get substantially accelerated once off-diagonal system–environment interactions are included. For the particular choice of C_{12} and C_{23}, the well-known sequential dynamics of the D–B–A model is closely mirrored, even for small electronic coupling [V_{DB} = 2 cm^{-1} and V_{BA} = 2 cm^{-1}, cf. Eq. (11)]. The decay of the initially populated donor state D is characterized by $\tau \approx 2.50$ ps.

Figure 2(c) presents the temperature dependence of the donor decay lifetime τ in the range 25 K–300 K. For the investigated cases of diagonal and non-diagonal system–environment interaction, we find a moderate enhancement of the transfer rate $k = 1/\tau$ upon lowering of the temperature with a ratio k(300 K)/k(25 K) ≈ 0.49. The observed weak temperature dependence reflects pseudo-activationless electron transfer reactions[10] being preserved for off-diagonal system–environment interactions. In this regime, nonadiabatic multiphonon electron transfer theory is applicable, and the strong coupling to the medium vibrational motion dominates the transfer process. The weak temperature dependence reflects the fact that the crossing of the nuclear potential surfaces along the reaction coordinate of the ET reaction occurs within the energy range of the donor state vibrational levels, and medium reorganization is fast compared to the timescale of the transfer process. In the considered temperature range, the memory time τ_M < 250 fs, while the timescale of system dynamics is $\tau \sim$ [1.1–2.4] ps.

The fast medium reorganization ($\tau_M \ll \tau$) indicates that the dynamics is governed by a non-adiabatic, close-to-Markovian process. We have investigated the influence of memory time τ_M on the transfer dynamics for constant reorganization energy λ_R (Fig. S.3 of the supplementary material). We find that for reduced memory time τ_M, the donor-to-bridge transfer dynamics is moderately slowed down, while the impact on the secondary bridge-to-acceptor transfer step is more pronounced. These findings resemble the findings from multi-state tight-binding models:[23,48] because intersite couplings are small compared to the energy gap, population dynamics is substantially affected by the bath dynamics and the non-equilibrium bath state can accelerate the population dynamics if the long-time system–bath memory time is taken into account (Δk_{max} = 32). Thus, the findings demonstrate the impact of non-Markovian long-time system–bath memory on charge transport dynamics in the considered overdamped transfer regime.

An understanding of the acceleration of dynamics in the sequential D–B–A model despite the small electronic couplings V_{ij} can be obtained by considering the system Hamiltonian H' in the transformed basis [Eqs. (15) and (16)]. The unitary transformation U, determined by off-diagonal system–bath interaction, induces substantial coupling elements V'_{DB} and V'_{BA} in the intermediate transformed basis while approximately retaining the energetics ($\epsilon_i \approx \epsilon'_i$). As a consequence, we observe acceleration of the sequential population dynamics induced by the off-diagonal system–bath interaction. The direct $|D\rangle \rightarrow |A\rangle$ transfer matrix element V'_{DA} remains negligible compared to the donor–acceptor energy gap, and thus, the direct pathway $|D\rangle \rightarrow |A\rangle$ is irrelevant. This mechanism is further corroborated by the moderate temperature dependence of the donor decay lifetime τ [Fig. 1(c)] that reflects the largely preserved energetics in the transformed basis $\Delta E_{DB} \approx \Delta E'_{DB} \approx \lambda_R$. For the considered diagonal and off-diagonal system–bath interaction cases, the largely preserved temperature dependence suggests that the dynamics proceeds via the sequential $|D\rangle \rightarrow |B\rangle \rightarrow |A\rangle$ pathway also for off-diagonal system–environment interaction.

2. The D–B–A model in asymmetric-Λ configuration ($\epsilon_D < \epsilon_B$ and $\epsilon_B - \epsilon_D \approx k_BT$)

Mutations allow tuning the energy of the bridge state in bacterial RC in a range −500 cm^{-1} < ϵ_B < 1000 cm^{-1}.[49] The decay

dynamics in the D–B–A model with asymmetric-Λ configuration with a thermally accessible bridge is presented in Fig. 3(a) for diagonal interaction with the environment ($\epsilon_D < \epsilon_B = +200$ cm^{-1}; data for $\epsilon_B = +300$ are given in Fig. S.2 of the supplementary material). The depopulation of the donor D is substantially decelerated compared to the sequential D–B–A model with $\epsilon_D > \epsilon_B$ due to thermal activation slowing down the transfer dynamics ($\tau \approx 7.78$ ps). For diagonal coupling to the environment, fast dynamics on a low-ps timescale (cf. Fig. 2) can only be achieved by substantially increased electronic couplings V_{DB} and V_{BD}.[22]

Considering off-diagonal coupling to the environment [$C_{12} \neq 0, C_{23} \neq 0$, Fig. 3(b)], substantially accelerated dynamics can be realized compared to the diagonal interaction case and the dynamics can closely resemble the sequential ET dynamics via a low-energy bridge ($\epsilon_D > \epsilon_B$, cf. Fig. 2). In particular, the characteristic time constant for depopulation of the donor state is nearly indistinguishable ($\tau = 2.36$ ps). Despite the moderate V_{DB} and V_{BA}, the off-diagonal component of the system–bath interaction can induce large electronic couplings V'_{DB} and V'_{BA} in the transformed basis, while the impact of basis rotation on the energetics is minor. Similarly, the direct coupling element V'_{DA} in transformed basis is negligible for the chosen configuration $C_{12} = 0.2$ and $C_{23} = -0.04$ ($V'_{DA} \lesssim 15$ cm^{-1}), and the dynamics proceeds via the sequential pathway $|D\rangle \rightarrow |B\rangle \rightarrow |A\rangle$. Consequently, the dynamics in the asymmetric-Λ D–B–A configuration with a thermally accessible bridge can potentially be fast in the presence of off-diagonal system–bath interactions. In this situation, the donor decay lifetime τ is insufficient to distinguish between the energetics of the asymmetric-Λ model with off-diagonal interactions and sequential ET proceeding via a low energy bridge state of the D–B–A system.

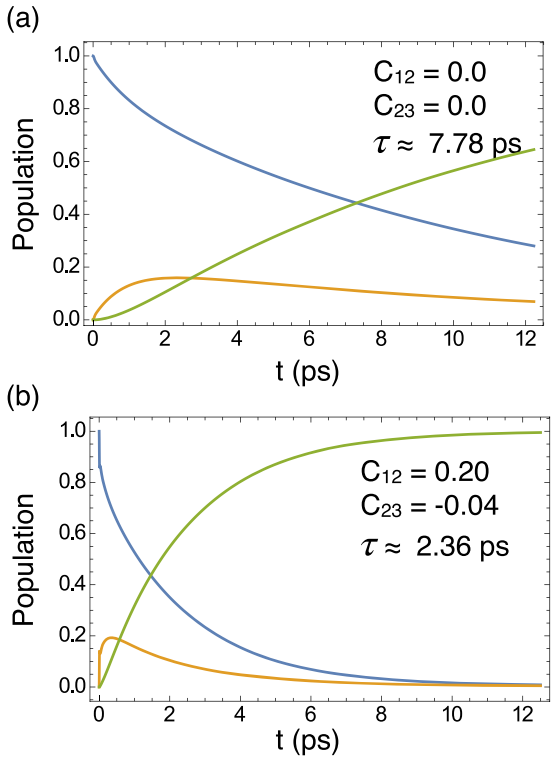

FIG. 3. Dynamics of the D–B–A model in asymmetric Λ configuration ($\epsilon_D = 0.0$, $\epsilon_B = +200$ cm$^{-1} > \epsilon_D$, and $\epsilon_A = -1000$ cm^{-1}) without (a) and with (b) off-diagonal system–environment interaction ($V_{DB} = 22$ cm^{-1} and $V_{BA} = 45$ cm^{-1}). Blue, orange, and green lines represent the populations of the donor state D, bridge state B, and acceptor state A, respectively. The dynamics with diagonal and off-diagonal system–environment interaction for $\epsilon_B = 300$ cm^{-1} are shown in Fig. S.2 of the supplementary material. Simulation parameters are summarized in Tables S.1–S.3 of the supplementary material, and see also Fig. S.3 for the impact of long-time system–bath memory on the dynamics.

The parameters d_1, d_2, and d_3 represent the relative strength of the fluctuation of the energy levels owing to the bath interactions. On the other hand, C_{12} and C_{23} denote the strength of fluctuation of the electronic couplings V_{DB} and V_{BA}, respectively. The simulations thus demonstrate that small off-diagonal contributions ($C_{ij} \ll d_1 - d_2$ or $d_2 - d_3$), i.e., non-Condon effects in V_{DB}, can substantially increase the effective coupling element and accelerate the dynamics. Here, the negative sign of C_{12} and/or C_{23} denotes the relative phase realized via anti-correlated fluctuations. Notably, correlated site energy and transfer coupling fluctuations have been predicted for the FMO light harvesting complex, while correlations of site energy fluctuations were found to be negligible.[41]

B. Off-diagonal induced superexchange transfer pathway $|D\rangle \rightarrow |A\rangle$

Variations of the D–B–A energetics in RC can be induced by point mutations that allow altering the relative importance of the sequential $|D\rangle \rightarrow |B\rangle \rightarrow |A\rangle$ and the direct, superexchange mediated pathway $|D\rangle \rightarrow |A\rangle$.[3,49] For the latter, transient population of the bridge is avoided, while the vibrational manifold of the bridge state mediates the transfer.[50] In the following, we consider a sequential D–B–A model ($\epsilon_D = 0$, $\epsilon_B = -150$ cm^{-1}, and $\epsilon_A = -1000$ cm^{-1}) for which with diagonal system–bath interactions, sequential bridge mediated transfer is the only pathway due to the absence of the direct coupling between the donor D and acceptor A ($V_{DA} = 0$, $V_{DB} = 22$ cm^{-1}, and $V_{BA} = 80$ cm^{-1}). In contrast, for non-diagonal interaction with the environment ($C_{12} = -0.089$, $C_{23} = 0.2$), the initially populated donor state D decays directly to the acceptor A. The negligible population of the bridge state B [Fig. 4(a)] suggests that the decay proceeds via a direct $|D\rangle \rightarrow |A\rangle$ channel, while the $|D\rangle \rightarrow |B\rangle \rightarrow |A\rangle$ channel is avoided. A similar scenario is realized in the asymmetric-Λ D–B–A model with non-diagonal coupling [$\epsilon_B = 400$ cm^{-1}, Fig. 4(b)] where transfer via the $|D\rangle \rightarrow |A\rangle$ channel is dominant and population of the bridge state B is avoided.

The predominance of the direct $|D\rangle \rightarrow |A\rangle$ channel is confirmed by the fact that the dynamics is largely independent of the energy of the bridge state [$\epsilon_B = -150$ cm^{-1} vs $\epsilon_B = 400$ cm^{-1}; cf. Figs. 4(a) and 4(b)]. Furthermore, the decay dynamics of the donor state D is largely independent of variations in temperature [$T = 100$ K–300 K; Fig. 4(c)], contrasting to the pseudo-activationless electron transfer reactions of the sequential D–B–A model (Fig. 2). In the latter scenario, the direct V'_{DA} coupling in transformed basis is negligible. The dominant $|D\rangle \rightarrow |A\rangle$ channel in the presence of non-diagonal system–environment interaction can arise in a transformed basis if the V'_{DA} coupling element becomes dominant, while coupling

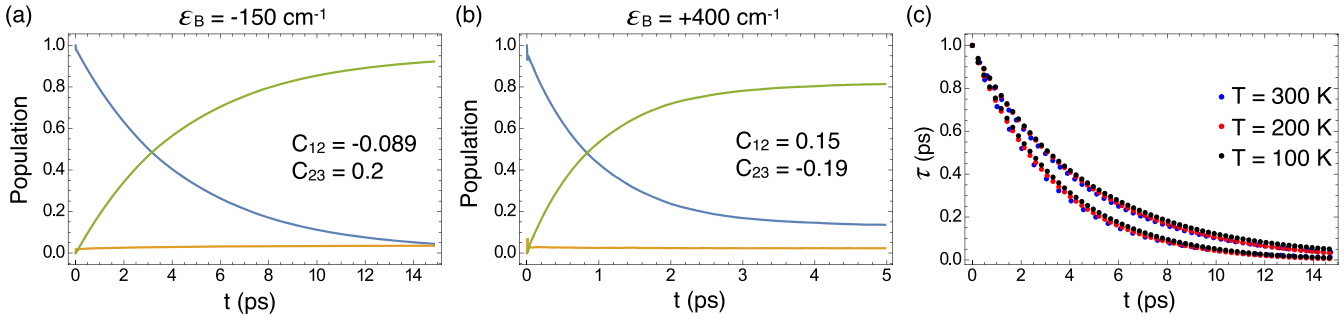

FIG. 4. Off-diagonal induced superexchange transfer pathway $|D\rangle \rightarrow |A\rangle$ for (a) the sequential D–B–A model (ϵ_D = 0.0, ϵ_B = −150 cm^{-1}, and ϵ_A = −1000 cm^{-1}) and (b) the D–B–A model in asymmetric Λ configuration (ϵ_D = 0.0, ϵ_B = +400 cm^{-1}, and ϵ_A = −500 cm^{-1}). Electronic couplings are V_{DB} = 22 cm^{-1} and V_{BA} = 80 cm^{-1} (a) and V_{DB} = 38 cm^{-1} and V_{BA} = 90 cm^{-1} (b). Blue, orange, and green lines represent the populations of the donor state *D*, bridge state *B*, and acceptor state *A*, respectively. (c) Population decay of the donor state *D* for various *T* in the setting of the sequential D–B–A model with off-diagonal induced superexchange pathway [(a) and (b)]. Simulation parameters are summarized in Tables S.1–S.3 of the supplementary material.

element of the direct pathway V'_{DB} becomes suppressed. Accordingly, the sequential population transfer via the bridge *B* is negligible, while the dominant transfer channel occurs from the donor to the acceptor $|D\rangle \rightarrow |A\rangle$.

1. Competition between sequential $|D\rangle \rightarrow |B\rangle \rightarrow |A\rangle$ and superexchange $|D\rangle \rightarrow |A\rangle$ transfer pathways

Starting from the generic sequential D–B–A model (ϵ_D = 0, ϵ_B = −150 cm^{-1}, and ϵ_A = −1000 cm^{-1}), we further investigate a scenario where both the sequential $|D\rangle \rightarrow |B\rangle \rightarrow |A\rangle$ and the superexchange mediated $|D\rangle \rightarrow |A\rangle$ transfer pathways contribute simultaneously to the dynamics (Fig. 5). We find that the presence of off-diagonal system–environment interactions can activate both transfer pathways, and the overall population decay of the donor state *D* becomes accelerated (characteristic time constant $\tau \approx 1.6$ ps compared to $\tau \approx 2.83$ ps for the diagonal system–bath interaction case). The observed behavior can again be rationalized by considering the Hamiltonian in the transformed basis [Eqs. (15) and (16)]. The particular unitary transformation induces couplings of comparable magnitude between all contributing states *D*, *B*, and *A* (V'_{DB} = −21.32 cm^{-1}, V'_{BA} = −85.96 cm^{-1}, and V'_{DA} = 114.24 cm^{-1}), while the energetics of the sequential D–B–A model is largely preserved (ϵ'_D = −16.72 cm^{-1}, ϵ_B = 147.1 cm^{-1}, and ϵ_A = −986.19 cm^{-1}). Due to the comparable magnitude of coupling elements V'_{DA} and V'_{BA}, the superexchange pathway $|D\rangle \rightarrow |A\rangle$ now competes with the $|D\rangle \rightarrow |B\rangle \rightarrow |A\rangle$ pathway. The off-diagonal system–bath interaction here operates by mediating the additional direct $|D\rangle \rightarrow |A\rangle$ decay channel, while at the same time, the dynamics of the sequential $|D\rangle \rightarrow |B\rangle \rightarrow |A\rangle$ pathway is preserved.

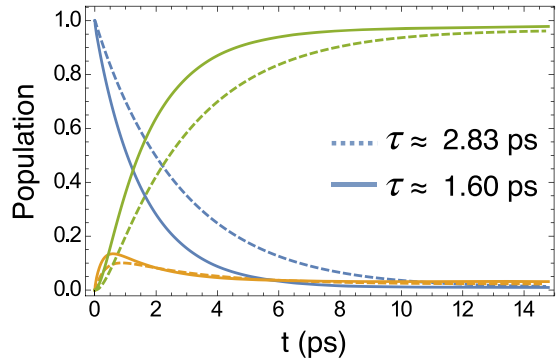

FIG. 5. Sequential $|D\rangle \rightarrow |B\rangle \rightarrow |A\rangle$ and super-exchange $|D\rangle \rightarrow |A\rangle$ pathway competition in the sequential D–B–A model (ϵ_D = 0.0, ϵ_B = −150 cm^{-1}, and ϵ_A = −1000 cm^{-1}). Dashed and solid lines denote simulations with diagonal ($C_{12} = C_{23} = 0$) and with off-diagonal (C_{12} = 0.08, C_{23} = 0.2) system–environment interaction, respectively (V_{DB} = 22 cm^{-1} and V_{BA} = 80 cm^{-1}). Blue, orange, and green lines represent the populations of donor state *D*, bridge state *B*, and acceptor state *A*, respectively. Simulation parameters are summarized in Tables S.1–S.3 of the supplementary material (see also Fig. S.3 for the impact of long-time system–bath memory on the dynamics).

C. Anomalous bridge localization

In the following, we discuss distinct scenarios of the sequential D–B–A model where off-diagonal system–bath interactions induce anomalous localization of population in the bridge state *B*.

1. Suppression of B–A population transfer

Anomalous localization in the bridge state *B* can be induced if off-diagonal interaction primarily affects the second $|B\rangle \rightarrow |A\rangle$ transfer step (C_{12} = 0.0 and C_{23} = 0.053; Fig. 6). Here, population transfer initially occurs from donor *D* to bridge *B* on the 2 ps–3 ps timescale, while the direct transfer pathway $|D\rangle \rightarrow |A\rangle$ is negligible. However, subsequent $|B\rangle \rightarrow |A\rangle$ transfer is suppressed in the particular off-diagonal system–environment configuration, and population acquired in the bridge *B* is thus unable to decay to the acceptor *A*. Figure 6 demonstrates that such anomalous localization in the bridge *B* can be realized with a small off-diagonal component particularly impacting the $|B\rangle \rightarrow |A\rangle$ dynamics ($C_{23} \neq 0$). The anomalous localization scenario is realized if in the transformed basis, the coupling element V'_{BA} is suppressed while V'_{DA} is very small (compared

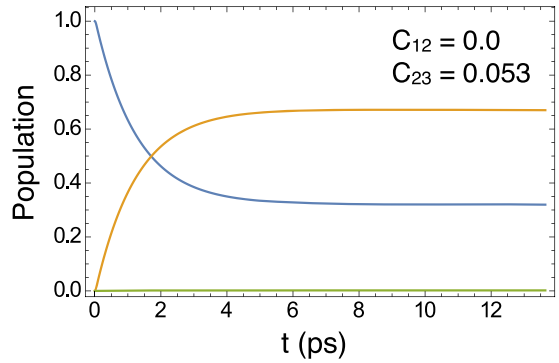

FIG. 6. Anomalous localization in the sequential D–B–A model (ϵ_D = 0.0, ϵ_B = −150 cm^{-1}, and ϵ_A = −1000 cm^{-1}) with electronic couplings V_{DB} = 22 cm^{-1} and V_{BA} = 45 cm^{-1}. Blue, orange, and green lines represent the populations of donor state *D*, bridge state *B*, and acceptor state *A*, respectively. Simulation parameters are summarized in Tables S.1–S.3 of the supplementary material.

to the donor–acceptor energy gap). As the bridge–acceptor coupling V'_{BA} is negligible, the population acquired in the bridge *B* is unable to decay to the acceptor state, and in the steady state, the bridge remains populated, while no population transfer to the acceptor is observed.

2. Anomalous bridge localization via renormalization of tunneling amplitudes

In the following, we demonstrate population localization in the bridge state *B* at a low temperature where the underlying mechanism exploits the renormalization of the tunneling amplitudes for (ultra-)strong interaction with the environment. For diagonal system–environment interaction, the localization of a two-level system (spin–boson model) strongly interacting with the environment is well understood.[24,51–53] The renormalization of tunneling amplitudes $V_{ij} \to 0$ induces a freezing of the dynamics and thus a persistent localization of population that manifests in the Berezinskii–Kosterlitz–Thouless (BKT) phase transition at the critical interaction strength α_c. How such environment induced localization is manifested in the presence of off-diagonal interactions with the environment for multi-level systems is largely unexplored.

Figure 7(a) shows the freezing of the population at the initial value due to tunneling amplitude renormalization induced by the strong diagonal interaction with the environment [$\alpha > \alpha_c \approx 1 + O(V_{DB}/\omega_c)$, dashed lines] at a low temperature (T = 0.05 K). The system is unable to decay via $|D\rangle \to |B\rangle \to |A\rangle$ if $\alpha|d_1 - d_2| > \alpha_c$ is satisfied, as $V_{DB} \to 0$. No condition for d_3 is required [$V_{DA} = 0$, Eq. (1)].

In the presence of off-diagonal system–bath interactions, significant differences to the diagonal interaction case are identified. The system exhibits overdamped decay dynamics toward the thermal equilibrium state if $\alpha|D_1 - D_2| > \alpha_c$ and $\alpha|D_2 - D_3| > \alpha_c$ but $\alpha|D_1 - D_3| < \alpha_c$ [solid lines in Fig. 7(a), with D_i being the eigenvalues of the system–environment interaction matrix, Eq. (14)]. Localization in the bridge *B* via a freezing of dynamics due to a renormalization of tunneling amplitudes ($V_{ij} \to 0$) is only observed if $\alpha|D_\alpha - D_\beta| > \alpha_c$ for all $\alpha \neq \beta$ ($\alpha, \beta = 1, 2, 3$) [Fig. 7(b)]. In analogy to the diagonal interaction case, the tunneling processes are suppressed due to tunneling amplitude renormalization, but initial short time dynamics persists, which determines the degree of localization.[54] Figure 7(c) presents the dynamics for $\alpha|D_1 - D_2| > \alpha_c$ and $\alpha|D_1 - D_3| > \alpha_c$, but $\alpha|D_2 - D_3| < \alpha_c$. In this scenario, population transfer between the donor *D* and bridge *B* is suppressed after the initial short time dynamics, but subsequent population transfer among the bridge *B* and the acceptor state *A* is facilitated.

In the presence of off-diagonal system–bath interactions, we thus identify distinct mechanistic differences for the anomalous population localization via the renormalization of tunneling amplitudes $V_{ij} \to 0$: (i) due to the basis transformation of initial conditions [Eq. (17)], coherences are imposed in the initial conditions that induce short time dynamics and consequently a population of all basis states $|D'\rangle$, $|B'\rangle$, and $|A'\rangle$, and (ii) stricter requirements are to be satisfied by the system–bath interactions in order to realize anomalous bridge localization due to a freezing of the dynamics, arising from the strong interaction in the BKT localized phase. For

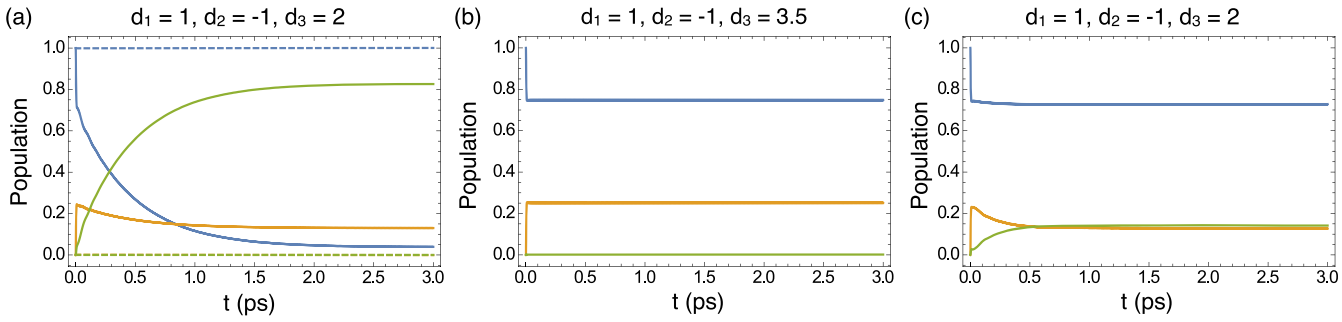

FIG. 7. Off-diagonal induced anomalous bridge localization at a low temperature (T = 0.05 K) via renormalization of tunneling amplitudes $V_{ij} \to 0$ in the sequential D–B–A model (ϵ_D = 0, ϵ_B = −100, and ϵ_A = −500; electronic couplings: $V_{DB} = V_{BA}$ = 20 cm^{-1}). Dashed and solid lines in (a) denote the cases with diagonal and off-diagonal system–environment interactions, respectively. Solid lines show the dynamics for the case $\alpha|D_1 - D_2| > \alpha_c$ and $\alpha|D_2 - D_3| > \alpha_c$ but $\alpha|D_1 - D_3| < \alpha_c$ [with D_i being the eigenvalues of the system–environment interaction matrix, Eq. (14)]. (b) Dynamics for the case $\alpha|D_1 - D_2| > \alpha_c$, $\alpha|D_2 - D_3| > \alpha_c$, and $\alpha|D_1 - D_3| > \alpha_c$. (c) Dynamics for the case $\alpha|D_1 - D_2| > \alpha_c$ and $\alpha|D_1 - D_3| > \alpha_c$ but $\alpha|D_2 - D_3| < \alpha_c$. Blue, orange, and green lines represent the populations of donor state *D*, bridge state *B*, and acceptor state *A*, respectively. Simulation parameters are summarized in Tables S.1–S.3 of the supplementary material.

example, the condition for the diagonal interaction case, $\alpha|D_1 - D_2| > \alpha_c$ with arbitrary D_3, is not sufficient because this only renormalizes V'_{DB} to zero but not V'_{DA} whose magnitude can become significant due to basis rotation. Thus, in the presence of non-diagonal system–bath interactions, the conditions for bridge localization are stricter: $\alpha|D_1 - D_2| > \alpha_c$, $\alpha|D_2 - D_3| > \alpha_c$, and $\alpha|D_1 - D_3| > \alpha_c$ need to be simultaneously satisfied to sufficiently renormalize V'_{BA} and V'_{DA}. Alternatively, when $\alpha|D_1 - D_2| > \alpha_c$ and $\alpha|D_1 - D_3| > \alpha_c$ but $\alpha|D_2 - D_3| < \alpha_c$ [Fig. 7(c)], the donor population freezes subsequent to the initial short-time dynamics as both V'_{DB} and V'_{DA} are renormalized to zero, which suppresses tunneling processes involving the donor state D but still facilitates equilibration between the bridge B and acceptor A.

D. Donor–acceptor coherence transfer

The prototypical dynamics in the sequential D–B–A model (Fig. 2) proceeds overdamped and is reasonably accounted for by pseudo-activationless non-adiabatic ET theory.[10–12] Accordingly, the timescales of population transfer and environment relaxation are largely separated, and non-Markovian environment relaxation has a modest impact on donor D and transient bridge B population (cf. Fig. S.3 of the supplementary material).[22] Nevertheless, in biological ET, where the sluggish protein matrix together with water fluctuations are of paramount importance, a close interplay between energy gap and transfer coupling element fluctuations is anticipated.[33] Such interplay is particularly permissible if the correlation time of site energies and transfer couplings is comparable to the time scale of the ET process. In our simulations of the transfer dynamics in the prototypical D–B–A model (Secs. III A and III B), energetics and magnitude of transfer couplings are chosen to resemble the dynamics of the bacterial RC[12,22,47] for which details of site energy and transfer coupling correlations have not been reported. Correlations of site energy and transfer coupling fluctuations have been proposed for the FMO light harvesting complex,[41] and non-Condon fluctuations of transfer couplings have been reported for the PE545 light harvesting complex[55] and for ET at oligothiophene–fullerene interfaces[29] where reported magnitudes of off-diagonal fluctuation are consistent with correlated off-diagonal system–environment interactions, $|C_{ij}| \lessapprox 0.2$.

In fact, the short-time pump–probe and 2D spectra of bacterial RC[13–16] show coherent, non-exponential dynamics that potentially arises from (ground or excited state) vibrational wavepackets, indicating comparable timescales of population transfer and environment relaxation. Of particular interest are coherent signatures at the spectral position indicative of the acceptor A (bacteriopheophytin H_A) that indicate the possibility of direct donor-to-acceptor coherence transfer. Recent 2D measurements suggest a scenario with more complex electronic and vibrational interactions within the first hundreds of femtoseconds in bacterial RC.[16]

In the following, we explore possibilities of coherent transfer dynamics between the donor D and acceptor A and the impact of non-diagonal system–environment interactions. Figure 8 presents the dynamics of a modified sequential D–B–A model with increased donor–bridge and bridge–acceptor coupling elements ($V_{DB} = 130$ cm^{-1} and $V_{BA} = 145$ cm^{-1}). For ease of numerical efficiency, we consider a reduced donor–acceptor energy gap ($\Delta(\epsilon_D - \epsilon_A) = 600$ cm^{-1} and $\epsilon_B = -100$ cm^{-1}). In the modified

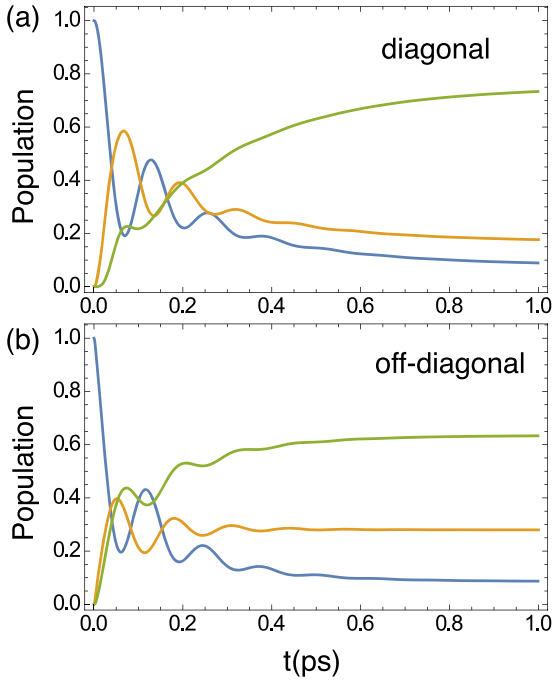

FIG. 8. Donor–acceptor coherence transfer in a sequential D–B–A model ($\epsilon_D = 0$ cm^{-1}, $\epsilon_B = -100$ cm^{-1}, and $\epsilon_A = -500$ cm^{-1} and electronic couplings: $V_{DB} = 130$ cm^{-1} and $V_{BA} = 145$ cm^{-1}) at room temperature ($T = 300$ K). The real time dynamics is shown for diagonal (a) and off-diagonal (b) system–environment interactions (system–environment interaction strength $\alpha = 0.835$). Off-diagonal system–environment interactions are $C_{12} = 0.2$ and $C_{23} = 0.9$ (b). Blue, orange, and green lines represent the populations of donor state D, bridge state B, and acceptor state A, respectively. Simulation parameters are summarized in Tables S.1–S.3 of the supplementary material.

setting, accelerated transfer dynamics occurs and the timescales of population transfer and environment relaxation become comparable. Accordingly, the population dynamics of the sequential D–B–A model shows coherent oscillatory modulations involving the donor D, bridge B, and acceptor A with diagonal system–environment interaction [Fig. 8(a); $C_{12} = C_{23} = 0$]. Oscillatory dynamics occurs on the few-hundred fs timescale and is followed by exponential equilibration dynamics occurring on the ≈1 ps timescale. Oscillations appear particularly pronounced in the donor and bridge population, while the acceptor population follows a step-function increase during the first ≈300 fs.

Off-diagonal system–environment interactions allow us to modulate the relative amplitudes of the oscillatory donor, bridge, and acceptor population dynamics [Fig. 8(b); $C_{12} = 0.2$ and $C_{23} = 0.9$]. In the particular realization, the oscillatory decay of the donor state D is largely preserved while the oscillation amplitude of the bridge state B is decreased and the oscillation amplitude of the acceptor state A is increased. Figure 9 presents the frequency domain representation of the dynamics for varying system–environment interaction strength α. We find that for increasing α, the non-zero frequency components (centered around ≈300 cm^{-1})

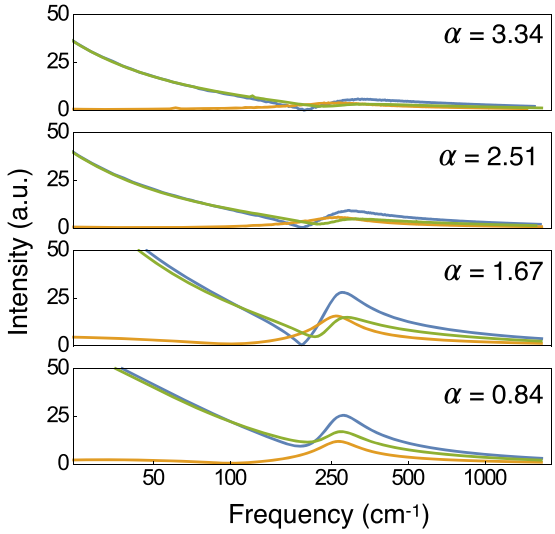

FIG. 9. Frequency domain representation of the oscillatory dynamics in a sequential D–B–A model for various values of the system–environment interaction strength α. Frequency domain data were obtained upon Fourier transform of the oscillatory dynamics for off-diagonal system–environment interactions (C_{12} = 0.2 and C_{23} = 0.9; see Fig. 8) after subtraction of the long-time equilibrium populations of the respective states. Blue, orange, and green lines represent the populations of the donor state *D*, bridge state *B*, and acceptor state *A*, respectively.

become weaker, while the zero frequency component increases, as expected for the transition from oscillatory to overdamped dynamics. While the peak position of the bridge state *B* is largely unaffected, the peak positions characterizing the coherent dynamics of the donor *D* and acceptor *A* states are slightly shifted to higher frequencies for increasing system–environment interaction strength α. The observed oscillation frequency is attributed (within ≈25 cm^{-1}) to the donor *D*–bridge *B* energy gap of the diagonalized Hamiltonian in the transformed basis (253 cm^{-1}). For weak-to-moderate interaction with the environment (α = 0.8–1.6), the oscillation frequency appears nearly unperturbed by the interaction with bath, while for strong system–bath interaction, deviations from the system Hamiltonian eigenvalues become larger (up to 60 cm^{-1}) due to a bath induced renormalization of system frequencies. Thus, upon increase in the system–environment interaction strength α (Fig. 9), the coherence frequency monotonically shifts away from the system resonance frequency to higher frequencies, and the amplitude of coherences is reduced due to increased interaction strength with the environment.

1. Donor-acceptor coherence transfer in the absence of electron transfer couplings

In the following, we numerically demonstrate that donor *D* to acceptor *A* coherence transfer can be induced via the off-diagonal interaction with the environment. For the purpose of demonstration, we consider a sequential D–B–A model (ϵ_D = 0, ϵ_B = −100 cm^{-1}, and ϵ_A = −500 cm^{-1}) that neglects the electronic coupling elements, which mediate the (coherent) transfer dynamics (V_{DB} = V_{BA} = 0). Thus, for diagonal system–bath interaction, the model does not show any dynamical time evolution.

Figure 10 demonstrates that in the presence of off-diagonal system–bath coupling ($C_{12} \neq C_{23} \neq 0$, $d_0 \neq 0$, $d_1 = d_2 = d_3 = d_0$), the short-time dynamics can become oscillatory. Most importantly, the simulations reveal that not only the donor *D* and bridge *B* populations but also the acceptor population shows coherent dynamics. The characteristic features of the oscillatory dynamics are distinct from coherent dynamics appearing at weak-to-intermediate

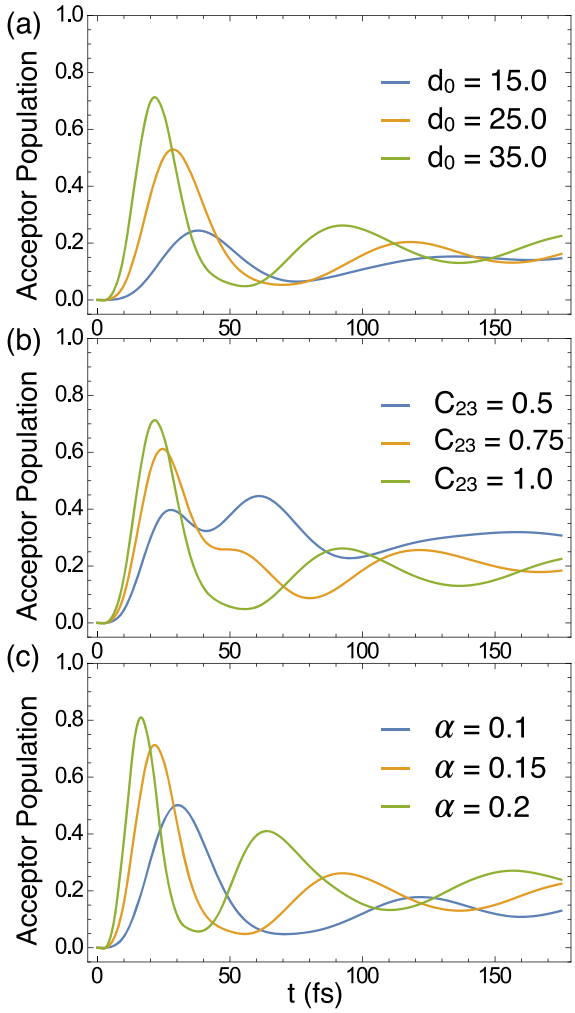

FIG. 10. Donor–acceptor coherence transfer in the sequential D–B–A model (ϵ_D = 0, ϵ_B = −100 cm^{-1}, and ϵ_A = −500 cm^{-1}; electronic coupling: V_{DB} = V_{BA} = 0) at strong system–environment interaction. (a) Oscillatory dynamics for variations of the bath displacement parameter d_0 (α = 0.15 and C_{12} = C_{23} = 1). (b) Oscillatory dynamics for variation of the off-diagonal system–environment interaction C_{23} (α = 0.15, C_{12} = 1, and d_0 = 35). (c) Oscillatory dynamics for variation of the system–environment interaction strength α (C_{12} = C_{23} = 1 and d_0 = 35). Diagonal entries of the system–environment interaction matrix are identical to the shift d_0 ($d_1 = d_2 = d_3 = d_0$), and simulation parameters are summarized in Tables S.1–S.3 of the supplementary material.

coupling to the environment (cf. Fig. 8). We find that the oscillation frequency and the amplitude of oscillations increase with growing values of the coupling strength α, the oscillator displacement d_0, and the magnitude of off-diagonal system–environment interactions C_{ij} [Figs. 10(a)–10(c)].

The oscillatory dynamics depicted in Fig. 10(a) reveals that the diagonal displacement parameter d_0 plays a crucial role in determining the short-time dynamics. This finding contrasts the dynamics in the D–B–A model with diagonal system–environment interaction ($C_{12} = C_{23} = 0$) where a constant diagonal shift d_0 of the coupling matrix $d_1 \to d_1 + d_0$, $d_2 \to d_2 + d_0$, and $d_3 \to d_3 + d_0$ does not affect the dynamics because the diagonal shift affects neither the coupling strength nor the tunneling amplitudes.[51] In the D–B–A model with non-diagonal system–bath interactions, the non-exponential short-time dynamics proceeding equilibration via tunneling processes is accelerated by the diagonal shift d_0, and oscillatory dynamics can be more pronounced (cf. also initial dynamics in Fig. 3).

The anomalous characteristics of the short-time dynamics can be understood from the canonical mapping between the D–B–A model with off-diagonal system–environment interactions and the vibronic interactions in the primary reaction coordinate model [Sec. II B and Eq. (4)]. The non-equilibrium electronic state couples (non-diagonally) to the primary mode that subsequently dissipates into a bath.[36] The finite non-Markovian relaxation timescale of the environment here creates a bottleneck for energy dissipation giving rise to the observed short-time coherences. The non-equilibrium excitation of the primary mode can be transferred back to electronic state that can become susceptible to re-excitation, which leads to the observed oscillatory coherent dynamics in the D–B–A model in the absence of electronic coupling elements. Accordingly, the ultrafast short-time dynamics is dominated by quantum effects and has negligible tunneling contributions. The observed short-time oscillation frequency becomes transparent in the primary reaction coordinate framework: the timescale of the short-time dynamics and hence the oscillations is determined by the energy scale ω_c. In the primary reaction coordinate model, ω_c is connected to the frequency of the primary oscillator Ω and its damping coefficient γ due to subsequent dissipation into the bath: $\omega_c = \Omega^2/\gamma$. For example, in the considered overdamped regime, a primary mode $\Omega \sim 500\ \mathrm{cm}^{-1}$ with $\gamma \sim 2500\ \mathrm{cm}^{-1}$ yields $\omega_c = 100\ \mathrm{cm}^{-1}$. A large oscillator displacement d_0 and off-diagonal coupling strength C_{ij} accelerate the transfer of excitation from the electronic state to the primary mode, thus enhancing non-equilibrium oscillatory vibronic features. The observed coherences (Fig. 10) have frequencies on the order ~400–800 cm^{-1} that persist for few hundreds of femtoseconds. The off-diagonal induced electronic coherent process thus survives well on the time scale of molecular vibrations and is readily observable with the available spectroscopic detection methods.[56,57]

IV. CONCLUSIONS

We have numerically demonstrated in non-perturbative QUAPI simulations that non-diagonal system–environment interactions can profoundly affect the observed dynamics in the prototypic D–B–A model. Off-diagonal induced acceleration of the dynamics has been demonstrated for the sequential D–B–A model with a low-energy bridge state and in asymmetric-Λ configuration. Additionally, we have shown how off-diagonal system–environment interactions can activate the direct superexchange transfer pathway. In all cases, the subtle deviations from cases with diagonal system–environment interaction preclude the assignment of a definitive transfer mechanism from the dynamics alone.

The suppression of bridge B to acceptor A population transfer mediated by the off-diagonal interaction with the environment allows for anomalous localization of population in bridge states. Two mechanisms of anomalous bridge B localization are identified where (i) due to basis transformation, the effective coupling element is suppressed and (ii) anomalous localization in the bridge state can be induced at a low temperature via a renormalization of tunneling amplitudes for strong interaction with the environment. In the latter case, more stringent criteria for localization are identified compared to the diagonal case via the underlying localization mechanism of the spin–boson model at strong interaction with the environment.

Coherence transfer between the donor D and acceptor A was demonstrated to be affected by the presence of off-diagonal system–environment interactions. The environment mediated D–A coherence transfer in the absence of electron transfer couplings exhibits anomalous characteristics for the short-time dynamics, i.e., an increase in the oscillation amplitudes with increasing system–environment interaction strength, oscillator displacement, and off-diagonal system–environment interactions. The characteristics become transparent upon the canonical mapping of the D–B–A model Hamiltonian with off-diagonal system–environment interactions onto the vibronic primary reaction coordinate model. Our results reveal a novel view on short-time coherent dynamics that arises from the complex and strong interaction of the environment and electronic degrees of freedom induced by vibronic non-Condon effects.

SUPPLEMENTARY MATERIAL

See the supplementary material for auxiliary dynamics of the sequential D–B–A model (Fig. S.1) and auxiliary dynamics of the D–B–A model in asymmetric Λ configuration (Fig. S.2), dependence of dynamics on memory times τ_M (Fig. S.3), Tables S.1–S.3 giving parameters of system Hamiltonians, bath and interaction Hamiltonians, and MACGIC-QUAPI settings used in simulations as well as numerical demonstration of convergence (Fig. S.4).

ACKNOWLEDGMENTS

B.P.F. acknowledges support by the DFG within the Emmy Noether Program (Grant No. FI 2034/1-1). This research received funding from the European Research Council (ERC) under the European Union's Horizon 2020 research and innovation program (Grant Agreement No. 802817).

DATA AVAILABILITY

The data that support the findings of this study are available from the corresponding author upon reasonable request.

REFERENCES

[1] A. Warshel and D. W. Schlosser, Proc. Natl. Acad. Sci. U. S. A. **78**, 5564 (1981).
[2] B. P. Fingerhut, W. Zinth, and R. de Vivie-Riedle, Phys. Chem. Chem. Phys. **12**, 422 (2010).
[3] M. Bixon and J. Jortner, J. Chem. Phys. **107**, 5154 (1997).
[4] A. Nitzan, Ann. Rev. Phys. Chem. **52**, 681 (2001).
[5] R. H. Goldsmith, M. R. Wasielewski, and M. A. Ratner, J. Phys. Chem. B **110**, 20258 (2006).
[6] B. P. Paulson, J. R. Miller, W.-X. Gan, and G. Closs, J. Am. Chem. Soc. **127**, 4860 (2005).
[7] T. C. Berkelbach, M. S. Hybertsen, and D. R. Reichman, J. Chem. Phys. **138**, 114103 (2013).
[8] Y. Guo, Z. Ma, X. Niu, W. Zhang, M. Tao, Q. Guo, Z. Wang, and A. Xia, J. Am. Chem. Soc. **141**, 12789 (2019).
[9] T. Arlt, S. Schmidt, W. Kaiser, C. Lauterwasser, M. Meyer, H. Scheer, and W. Zinth, Proc. Natl. Acad. Sci. U. S. A. **90**, 11757 (1993).
[10] M. Bixon and J. Jortner, Chem. Phys. Lett. **159**, 17 (1989).
[11] P. Huppmann, S. Spörlein, M. Bibikova, D. Oesterhelt, J. Wachtveitl, and W. Zinth, J. Phys. Chem. A **107**, 8302 (2003).
[12] B. P. Fingerhut, W. Zinth, and R. de Vivie-Riedle, Chem. Phys. Lett. **466**, 209 (2008).
[13] M. H. Vos, F. Rappaport, J.-C. Lambry, J. Breton, and J.-L. Martin, Nature **363**, 320 (1993).
[14] S. Spörlein, W. Zinth, and J. Wachtveitl, J. Phys. Chem. B **102**, 7492 (1998).
[15] V. I. Novoderezhkin, A. G. Yakovlev, R. van Grondelle, and V. A. Shuvalov, J. Phys. Chem. B **108**, 7445 (2004).
[16] F. Ma, E. Romero, M. R. Jones, V. I. Novoderezhkin, and R. van Grondelle, Nat. Commun. **10**, 933 (2019).
[17] M. Tanaka and Y. Tanimura, J. Phys. Soc. Jpn. **78**, 073802 (2009).
[18] M. Tanaka and Y. Tanimura, J. Chem. Phys. **132**, 214502 (2010).
[19] T. Kramer, M. Rodríguez, and Y. Zelinskyy, J. Phys. Chem. B **121**, 463 (2017).
[20] N. Lambert, S. Ahmed, M. Cirio, and F. Nori, Nat. Commun. **10**, 3721 (2019).
[21] N. Makri, E. Sim, D. E. Makarov, and M. Topaler, Proc. Natl. Acad. Sci. U. S. A. **93**, 3926 (1996).
[22] E. Sim and N. Makri, J. Phys. Chem. B **101**, 5446 (1997).
[23] M. Richter and B. P. Fingerhut, J. Chem. Phys. **146**, 214101 (2017).
[24] A. Strathearn, P. Kirton, D. Kilda, J. Keeling, and B. W. Lovett, Nat. Commun. **9**, 3322 (2018).
[25] N. Makri, J. Chem. Phys. **152**, 041104 (2020).
[26] M. Richter and B. P. Fingerhut, Faraday Discuss. **216**, 72 (2019).
[27] R. F. Goldstein, S. Franzen, and W. Bialek, J. Phys. Chem. **97**, 11168 (1993).
[28] A. Milischuk and D. V. Matyushov, J. Chem. Phys. **118**, 5596 (2003).
[29] H. Tamura, R. Martinazzo, M. Ruckenbauer, and I. Burghardt, J. Chem. Phys. **137**, 22A540 (2012).
[30] Y. Yao, N. Zhou, J. Prior, and Y. Zhao, Sci. Rep. **5**, 14555 (2015).
[31] M. G. Mavros, D. Hait, and T. Van Voorhis, J. Chem. Phys. **145**, 214105 (2016).
[32] P. Nalbach, I. Pugliesi, H. Langhals, and M. Thorwart, Phys. Rev. Lett. **108**, 218302 (2012).
[33] S. S. Skourtis, D. H. Waldeck, and D. N. Beratan, Ann. Rev. Phys. Chem. **61**, 461 (2010).
[34] A. Garg, J. N. Onuchic, and V. Ambegaokar, J. Chem. Phys. **83**, 4491 (1985).
[35] L. A. Correa, B. Xu, B. Morris, and G. Adesso, J. Chem. Phys. **151**, 094107 (2019).
[36] V. Chernyak and S. Mukamel, J. Chem. Phys. **105**, 4565 (1996).
[37] N. Makri and D. E. Makarov, J. Chem. Phys. **102**, 4611 (1995).
[38] E. Sim and N. Makri, Comput. Phys. Commun. **99**, 335 (1997).
[39] E. Sim, J. Chem. Phys. **115**, 4450 (2001).
[40] Z. Lü, L. Duan, X. Li, P. M. Shenai, and Y. Zhao, J. Chem. Phys. **139**, 164103 (2013).
[41] C. Olbrich, J. Strümpfer, K. Schulten, and U. Kleinekathöfer, J. Phys. Chem. B **115**, 758 (2011).
[42] P. Nalbach, N. Klinkenberg, T. Palm, and N. Müller, Phys. Rev. E **96**, 042134 (2017).
[43] S. Krempl, W. Domcke, and M. Winterstetter, Chem. Phys. **206**, 63 (1996).
[44] T. Palm and P. Nalbach, J. Chem. Phys. **149**, 214103 (2018).
[45] W. Domcke, D. R. Yarkony, and H. Köppel, *Conical Intersections*, Advanced Series in Physical Chemistry (World Scientific, 2004).
[46] V. Romero-Rochin and I. Oppenheim, Physica A **155**, 52 (1989).
[47] B. P. Fingerhut and S. Mukamel, J. Phys. Chem. Lett. **3**, 1798 (2012).
[48] R. Lambert and N. Makri, Mol. Phys. **110**, 1967 (2012).
[49] M. Bixon, J. Jortner, and M. E. Michel-Beyerle, Chem. Phys. **197**, 389 (1995).
[50] We adopt the definition of Ref. 3 where a superexchange mechanism is reflected in a vanishing transient population of the bridge *B*. This definition differs from Ref. 58 where the superexchange mechanism is mediated by the off-diagonal elements of the density matrix.
[51] U. Weiss, *Quantum Dissipative Systems*, 4th ed. (World Scientific, Singapore, 2012).
[52] S. Chakravarty, Phys. Rev. Lett. **49**, 681 (1982).
[53] A. J. Bray and M. A. Moore, Phys. Rev. Lett. **49**, 1545 (1982).
[54] N. Acharyya, M. Richter, and B. P. Fingerhut, arXiv:2009.12296 (2020).
[55] M. Aghtar, U. Kleinekathöfer, C. Curutchet, and B. Mennucci, J. Phys. Chem. B **121**, 1330 (2017).
[56] M. Liebel, C. Schnedermann, T. Wende, and P. Kukura, J. Phys. Chem. A **119**, 9506 (2015).
[57] M. Kowalewski, B. P. Fingerhut, K. E. Dorfman, K. Bennett, and S. Mukamel, Chem. Rev. **117**, 12165 (2017).
[58] S. S. Skourtis and S. Mukamel, Chem. Phys. **197**, 367–388 (1995).